

Porous amorphous carbon models from periodic Gaussian chains of amorphous polymers

Amit Kumar, Raul F. Lobo, Norman J. Wagner *

Colburn Laboratory, Department of Chemical Engineering, University of Delaware, 150 Academy Street, Newark, DE 19716, USA

Received 25 March 2005; accepted 21 June 2005

Available online 3 August 2005

Abstract

An algorithm has been developed to create structural models for amorphous carbons using Monte Carlo simulations in the canonical ensemble. The simulation method used follows the experimental preparation of nanoporous carbons (NPC) by pyrolysis from polyfurfuryl alcohol as a guideline. The resulting structure exhibits properties that compare favorably to those observed experimentally for real NPCs. These atomistic NPC models are approaching a realistic representation of NPCs used for gas separations and as such, are being used to study the diffusion of small gas molecules in these materials. Limitations of the method and possible improvements are discussed.

© 2005 Elsevier Ltd. All rights reserved.

Keywords: Porous carbon; Pyrolysis; Molecular simulation; Transport properties; Microstructure

1. Introduction

Several amorphous carbons have high surface area and porosity making them useful in separation and purification processes. Activated carbons, for example, are used in water purification, sugar refining and most relevant for this work, gas separation. Amorphous carbons can be broadly classified into graphitizing and non-graphitizing carbons [1]; the former usually transform to graphite when treated at high temperatures while the latter do not. Non-graphitizing carbons prepared from the pyrolysis of carbon containing polymeric precursors, such as polyfurfuryl alcohol (PFA) (structure shown in Fig. 1), are characterized by very high surface areas and narrow pore size distributions. These carbons are known as nanoporous carbons (NPC) and are important materials with applications in gas purification, as adsorbents and as catalyst supports [2–4]. NPCs

are used extensively in the pressure swing adsorption process to separate nitrogen and oxygen [5]. Membranes prepared from NPCs have been shown to exhibit nitrogen-to-oxygen selectivity values as high as 30:1 [6].

Despite being of importance in industry, there is no accepted atomistic model for NPCs. Pair distribution functions (PDF) obtained from neutron scattering experiments on NPCs show that these materials have structural correlations up to around 2 nm but are globally amorphous [7]. Adsorption studies indicate a very narrow pore size distribution for NPCs, the mean pore size being about 5 Å [2,8]. High resolution transmission electron microscopy (HRTEM) images of NPCs reveal the presence of curved graphene sheets in the structure [9–11]. The curvature is generally attributed to the presence of non-hexagonal rings in the structure. A good knowledge of the molecular structure of NPCs is vital to understanding the interesting separations possible with these materials.

Modeling the structure of amorphous materials is challenging. Two kinds of approaches are generally followed to model amorphous materials: mimetic and

* Corresponding author. Tel.: +1 302 831 8079; fax: +1 302 831 1048.

E-mail address: wagner@che.udel.edu (N.J. Wagner).

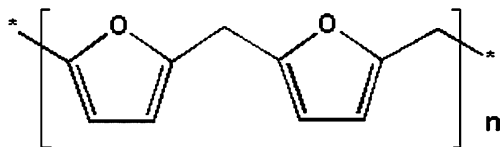


Fig. 1. Schematic diagram of the structure of polyfurfuryl alcohol.

reconstruction methods. Mimetic techniques simulate the process by which the material is synthesized experimentally and hence, require knowledge of the mechanism by which the material is formed. Gelb and Gubbins [12] used a mimetic simulation protocol to model the structure of Vycor glasses. Classical and ab initio molecular dynamics (MD) simulations are generally used to model amorphous materials using the mimetic approach [13,14]. On the other hand, reconstruction methods like reverse Monte Carlo (RMC) [15] refine an initial structure by moving the atoms so that the structure finally resembles the actual structure in terms of some experimentally observable property of the material (such as the PDF). A number of amorphous materials such as amorphous carbons [16,17], silica glasses [18] and other disordered materials [19–21] have been modeled using RMC.

Several previous attempts have been reported to model the structure of NPCs. Warren [22] showed the presence of layer-planes of graphite-like structure in a non-crystalline carbon (carbon black). It was observed [23] that the layers of graphitic domains were translationally and rotationally disordered, an arrangement known as turbostratic. Franklin [1] was the first to distinguish between graphitizing and non-graphitizing carbon, suggesting that the structure of non-graphitizing carbon consisted of randomly oriented graphite-like layers interconnected by non-organized carbon. However, recent HRTEM observations on non-graphitizing carbons [9,10] indicate the presence of curvature in the structure which necessitates more sophisticated models that account for the presence of non-hexagonal rings. Harris and Tsang [10] proposed a model for NPC structure in which curved fragments obtained from fullerenes were used as the building blocks. This model accounted for the presence of curvature and five-membered rings in the structure. Acharya et al. [24] attempted to generate the structure of NPC by connecting fragments of graphene sheets in a random fashion. This method was computationally inexpensive and could generate large models with non-hexagonal rings but the models generated were non-periodic. Smith et al. [25] randomly incorporated small amount of non-hexagonal rings into graphene sheets and turbostratically layered several such sheets to create a three dimensional model of NPC. RMC methods have also been used extensively to generate structural models for NPC. Thomson and Gubbins [16] used RMC on a starting structure of graphitic sheets

to generate a model for NPC. The models generated use graphite as the starting structure which is not the case for real NPCs. Rosato et al. [26] have used the RMC technique to generate amorphous carbon structures which they subsequently relaxed using tight binding molecular dynamics simulations. However, their investigations were limited to high density ($\rho = 3 \text{ g/cm}^3$) cases. Pikunic et al. [17] used RMC in conjunction with simulated annealing to generate models whose PDF matched the PDF of real NPCs very well. However, the models generated by RMC have the problem of non-uniqueness associated with them. Detailed review of the various methods used to model NPC structure can be found in articles by Harris [27] and Bandosz et al. [28].

In this paper, we present a novel algorithm for the development of NPC structures by mimetic pyrolysis. Canonical ensemble Monte Carlo (MC) simulations are used to evolve an initial polymer structure to an NPC. This new algorithm generates periodic carbon structures with pre-defined carbon density. The PDFs of the model structures generated using this method are found to match the experimental PDF of NPCs that show exceptional O_2/N_2 gas selectivity.

2. Simulation method

NPCs are commonly prepared in the laboratory by the pyrolysis of a carbon containing polymer precursor such as PFA [29,30]. Using this as a broad guideline, an NVT Monte Carlo (MC) simulation was developed starting with PFA to generate model amorphous carbon structures.

2.1. Generation of starting polymer

To generate the starting polymer, a technique proposed by Kotelyanskii et al. [31] was followed because this method guarantees linear polymers that are periodic, follow Gaussian statistics and fill space. The backbone of the polymer chain was generated on a completely filled cubic lattice (Fig. 2(a)), decorated with the repeat units and annealed using energy minimization to remove any structural overlaps. All the non-carbon atoms (i.e., hydrogen and oxygen) were then removed from the polymer structure and this polymer (devoid of all the non-carbon atoms) was used in the MC simulations as the starting structure. An example of such a starting structure folded inside a cubic periodic box is shown in Fig. 2(b).

A $7 \times 7 \times 7$ cubic lattice (having 343 node points) (see Fig. 2(a)) was used to generate the initial polymer backbones for all the models presented in this work. Simulations on polymer backbones generated on $9 \times 9 \times 9$ and $11 \times 11 \times 11$ lattices were also performed to explore the effect of lattice size on the final structure obtained.

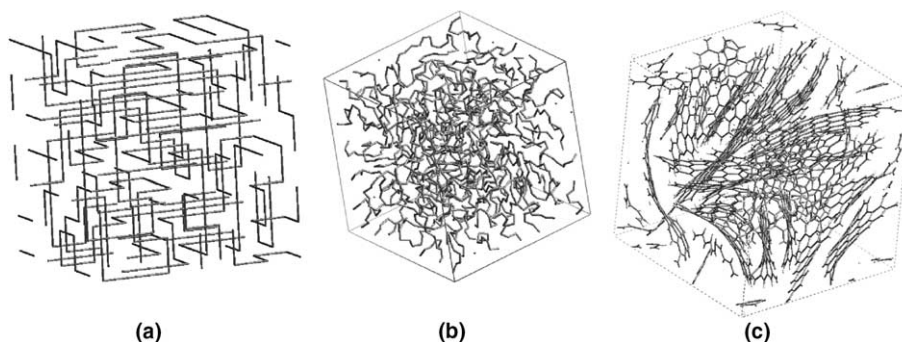


Fig. 2. Evolution of the structure during the simulation from an amorphous, Gaussian polymer backbone folded into a periodic simulation box to a folded linear carbon polymer to a disordered carbon structure with sp^2 coordination. (a) Polymer backbone on a $7 \times 7 \times 7$ cubic lattice, (b) starting polymer structure folded into a cubic simulation box and (c) final structure obtained after 4000 MC cycles at $T = 800$ °C and $\rho = 1.72$ g/cm³. For clarity, bonds crossing the periodic boundary have not been shown in any of the cases.

The results were found to be similar to those obtained for simulations carried out on a $7 \times 7 \times 7$ lattice under the same conditions.

2.2. Generation of NPC structure

The NVT MC simulations were carried out in a cubic simulation box with periodic boundary conditions. The DREIDING force field [32] was used to describe the bond stretching, bond bending, torsional and non-bonded interactions between the atoms. A Morse potential was used to model the bond stretching energy while a simple 12–6 Lennard–Jones (LJ) potential was used to model the non-bonded energy. Non-bonded interactions were not considered between atoms interacting by the bond stretching, bond bending or torsional interactions. Further, non-bonded interactions were not considered to be present between carbon atoms which were bonded to less than three other carbon atoms. For these atoms, if they were not already interacting with either bond stretching or bond bending or torsional interactions, a hard sphere potential was used. Two kinds of MC moves were carried out on the atoms.

- Move 1: Standard Metropolis MC was applied [33]. The maximum step size was 0.2 Å.
- Move 2: Atoms, selected at random, were given a large random displacement (maximum step size = 3.82 Å). After an atom was moved, all its bonds were broken, as well as all bonds of all the atoms within 2.65 Å of the new position of the moved atom. All the atom pairs involved in the bonds that were broken were stored in an array along with the atom pairs between which new bonds could form. Bonds were then reformed in random order between every stored atom pair under the following constraints:
 - The atoms involved in the formation of a bond could have a maximum of three bonded neighbors (because all carbon atoms are assumed to be sp^2 hybridized).

- A random number R was generated between 0 and 1. To accept the bond formation, this number had to be less than the probability P given by

$$P = \frac{e^{-E_{ab}/k_B T}}{1 + e^{-E_{ab}/k_B T}} \quad (1)$$

where k_B is the Boltzmann constant, T is the temperature at which the simulation is being carried out. E_{ab} is given by

$$E_{ab} = \frac{1}{2} K_e (r_{ab} - r_e)^2 - D \quad (2)$$

Here, r_{ab} is the distance between atoms a and b , r_e is the equilibrium bond distance, and K_e and D are constants chosen for the harmonic function E_{ab} to match the Morse potential (see Table 1). Finally, all the atoms involved in bond rearrangement were annealed using standard MC (50 moves with a maximum step size of 0.1 Å). Fig. 3 shows a schematic of the different steps involved in this type of move.

Both types of moves were accepted or rejected based on the Metropolis acceptance criterion. For every move, a random number \mathcal{R} was generated between 0 and 1 and compared to the Boltzmann factor $e^{-\Delta E/k_B T}$. If \mathcal{R} was less than or equal to the Boltzmann factor, the move was accepted, otherwise it was rejected. Here ΔE is the total energy change associated with the move. In the simulation, one step of type 2 was carried out after every 200 steps of type 1. One step of any type was complete

Table 1
Parameters used in the MC simulations to match the harmonic potential to the Morse potential

Parameter	Value
r_e	1.4 Å
K_e	700 kcal/(mol Å ²)
D	70 kcal/mol

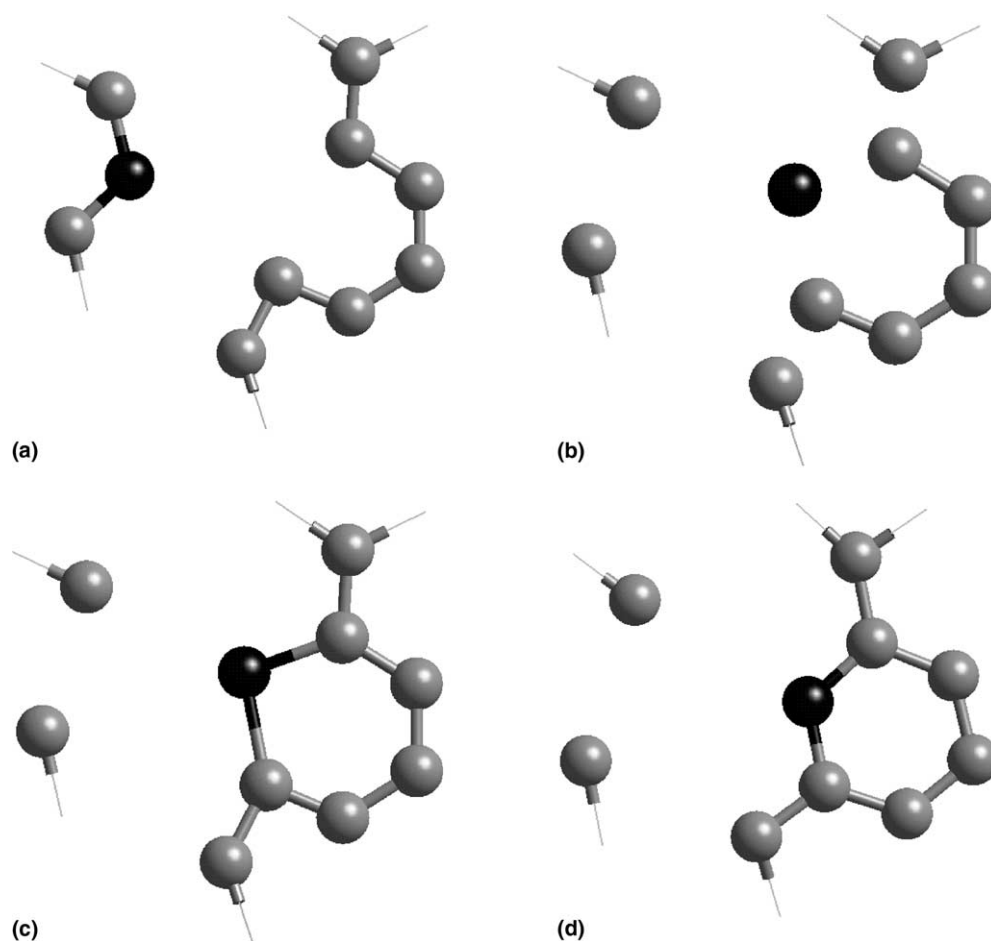


Fig. 3. Schematic of a MC move of type 2 (bond rearrangement). Atom being moved is shown in black. (a) Configuration before the move, (b) atom moved and bonds broken, (c) bonds formed back and (d) atoms involved in bond rearrangement equilibrated by MC.

when all the atoms in the system had been displaced once. The atoms to be displaced in a step were chosen in random order and no atom was displaced more than once in a step. One MC cycle is defined as a collection of 200 steps of type 1 and one step of type 2.

After the Monte Carlo simulations were complete, an optimized structure composed entirely of carbon atoms (some of which had less than three bonded neighbors) was obtained. To satisfy the coordination requirements of all the carbon atoms, hydrogen atoms were explicitly introduced into the structure using Cerius² software [34]. Energy minimization was subsequently carried out on the structure to remove any non-bonded overlaps.

The programs for the simulation were written in C++. The simulations were carried out on Linux machines with 2.4 GHz Intel Xeon processors. The simulation of a system (4000 MC cycles) having 1450 atoms at a temperature of 800 °C and density of 1.72 Å required approximately 20 days of computer time. The simulations were stopped after 4000 MC cycles because the fraction of carbon atoms bonded to three carbon atoms was generally seen to change by less than 1% between 3000 and 4000 MC cycles.

3. Characterization methods

The quality of the model carbon structure obtained was ascertained by comparing the pair distribution function (PDF), bond length and bond angle distribution, fraction of 5-, 6- and 7-membered rings and the composition (fraction of carbon atoms bonded to three carbon atoms). The final structures obtained from the simulations were further characterized by using the following metrics:

3.1. Pair Distribution Function (PDF), $g(r)$

This is the probability of finding two atoms a distance r apart relative to the probability expected for a complete random distribution at the same density. The PDF obtained from the simulations is defined as [33]

$$g^{\text{sim}}(r) = \rho^{-2} \left\langle \sum_i \sum_{j \neq i} \delta(\mathbf{r}_i) \delta(\mathbf{r}_j - \mathbf{r}) \right\rangle$$

$$= \frac{V}{N^2} \left\langle \sum_i \sum_{j \neq i} \delta(\mathbf{r} - \mathbf{r}_{ij}) \right\rangle \quad (3)$$

where ρ is the number density, $\delta(\dots)$ is the Dirac delta function, V is the volume of the system and N is the number of atoms in the system.

The experimental PDF used to compare with the models is given by [7]

$$g^{\text{expt}}(r) = \frac{2}{\pi} \int_0^\infty Q[S(Q) - 1] \sin(Qr) dQ \quad (4)$$

where Q is the magnitude of the scattering vector and $S(Q)$ is the structure factor. $g^{\text{expt}}(r)$ is related to $g^{\text{sim}}(r)$ through the following relationship (obtained by using equations in [35]).

$$g^{\text{expt}}(r) = 4\pi r \rho [g^{\text{sim}}(r) - 1] \quad (5)$$

The simulated PDF is transformed using equation (5) to compare with the experimental PDF.

3.2. Cavity size distribution and excluded volume map

The cavity size distribution (CSD) is defined as the probability distribution of inserting a hard-sphere probe into the structure without any overlaps between the probe and the atoms in the structure. In this work, the method described by Cuthbert et al. [36] was used for the calculation of CSDs. The simulation box was divided into a three-dimensional grid with adjacent node points 0.1 Å apart. At every node, the largest possible hard-sphere probe was then inserted. Finally, the distribution was binned and normalized.

The excluded volume map (EVM) is defined as a map of the volume elements in the structure where a hard-sphere probe of a given radius can be inserted without any overlaps with the structural atoms. To generate the EVMs, a three dimensional grid was placed on the simulation box and attempt was made to introduce the probe at all the different nodes of the grid. The node points where the placement of the probe did not result in any overlaps defined the EVM for the structure and the probe molecule. Hard sphere probes with diameters corresponding to single LJ site models for He, O₂ and N₂ were used as probes.

3.3. Bond anisotropy map

The degree of anisotropy in a structure is quantified by the net orientation of C–C bonds. Two-dimensional bond anisotropy contour maps were generated by recording all bond orientations in terms of the θ and ϕ angles in spherical coordinates. Thus, a bond density distribution was obtained as a function of the two spherical angles (θ and ϕ) relative to the Eulerian simulation box coordinates.

3.4. Simulation of transmission electron microscopy (TEM) images

TEM images of the model carbons were obtained using HRTEM module of the Cerius² software [34].

The images were generated at an electron energy of 200 kV and an aperture focus of 0.70 Å⁻¹. A defocus of –825 Å was used with a defocus spread of 250 Å. The spherical aberration coefficient and beam spread were 2.70 mm and 0.30 mrad respectively.

4. Results and discussion

Several simulations were carried out at various conditions to explore the effects of process as well as simulation parameters on the final structure. Temperature, density, simulation box size and the starting structure were varied (see Table 2). In Table 3, the fraction of 5-, 6- and 7-membered rings in the final structures obtained for the different simulations are listed. In all cases, the majority of the rings are hexagonal with 10–15% non-hexagonal rings present.

Fig. 2(c) shows the final structure obtained after 4000 MC cycles on a starting polymer structure at a temperature of 800 °C, density of 1.72 g/cm³ and cubic

Table 2

List of simulations performed along with the conditions at which they were carried out

	Starting structure	Temperature (°C)	Density (g/cm ³)	Simulation box size (Å)	Number of carbon atoms
1	Polymer A	800	1.72	25.68	1450
2	Polymer B	800	1.72	25.68	1450
3	Free carbon gas	800	1.72	25.68	1450
4	Polymer A ^a	800	1.72	25.68	1450
5	Polymer A	400	1.72	25.68	1450
6	Polymer A	1200	1.72	25.68	1450
7	Polymer A	800	1.38	25.68	1165
8	Polymer A	800	2.20	25.68	1855
9	Polymer A	800	1.72	28.59	2000
10	Polymer A	800	1.72	30.79	2500

Polymers A and B were created from two different configurations of the lattice polymer backbone.

^a The random number generation sequence in this case was different from case 1.

Table 3

Fraction of 5-, 6- and 7-membered rings in the final structures generated at different conditions (outlined in Table 2)

Simulation	% of 5-member rings	% of 6-member rings	% of 7-member rings	Total number of rings
1	7.0	86.9	6.1	443
2	6.9	89.0	4.1	435
3	5.1	91.2	3.7	429
4	6.2	88.8	5.0	439
5	6.5	90.1	3.4	414
6	5.8	89.4	4.8	451
7	7.9	86.7	5.4	353
8	4.4	91.5	4.1	539
9	6.3	87.8	5.9	605
10	6.9	88.8	4.3	723

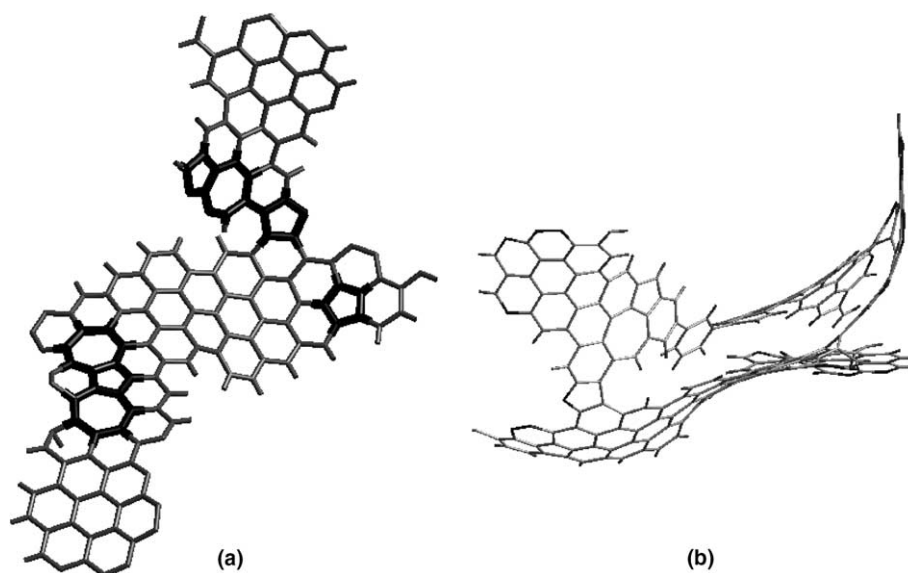


Fig. 4. “Defects” in the structure of the model carbons. The simulation was carried out at a temperature of 800 °C and a density of 1.72 g/cm³ in a cubic simulation box of length 25.68 Å and having 1450 carbon atoms. (a) A fragment of the final structure showing the presence of 5- and 7-membered rings and (b) a portion of the model carbon showing a “hole” in the structure.

simulation box length of 25.68 Å. The structure is composed of slightly curved, randomly-oriented graphene sheets. A section of this final structure is shown in Fig. 4(a) where the 5- and 7-membered rings are highlighted. The presence of non-hexagonal rings in the model structures is in conformity with experimental reports in literature [24]. Fig. 4(b) shows another “defect” found in this structure. A random interconnection of three carbon sheets produces what can be considered as a “hole” in the structure. Apart from the fraction of non-hexagonal rings, the structure was characterized using various other metrics like the bond length and bond angle distribution, fraction of hydrogen atoms, PDF, CSD, EVM and bond anisotropy map.

In Fig. 5, the variation of the fraction of carbon atoms bonded to 1, 2 and 3 carbon atoms as the simulation progresses is shown (the curves corresponding to polymer A). The rates of change of these fractions become very low after approximately 1000 MC cycles and the structure remains constant by the end of the simulation. This suggests that the final structure is trapped into a local free energy minimum. In the final structure, the fractions of carbon atoms bonded to 1, 2 and 3 carbon atoms are about 0%, 28% and 72% respectively, implying that the fraction of hydrogen atoms in the structure is about 22%, a value that is significantly higher than that observed experimentally in NPCs of the same density. This high hydrogen fraction is the result of a lower level of

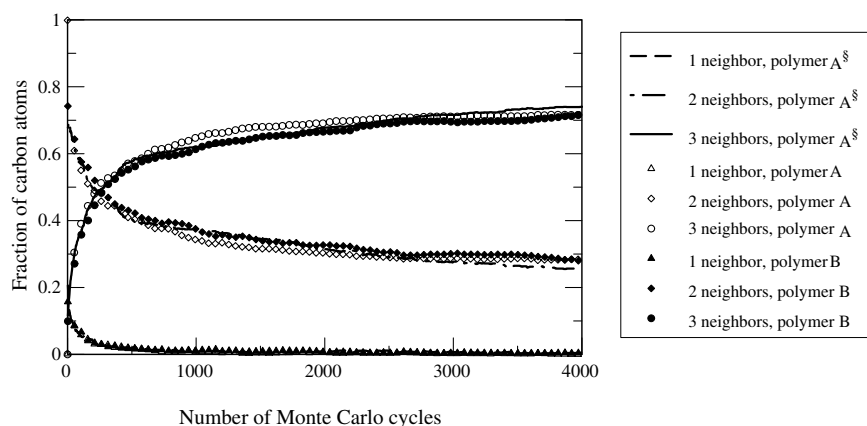


Fig. 5. Variation in the fraction of carbon atoms having different number of neighbors with the number of MC cycles. The simulations shown here were carried out at a temperature of 800 °C and a density of 1.72 g/cm³ in a cubic simulation box of length 25.68 Å and having 1450 carbon atoms. The three cases differ in the starting structure and the random number generation sequence. §Random number generation sequence in this case was different.

connectivity in the model carbons than in real carbons. For reference, pure graphite has 100% carbon atoms, all bonded to three other carbon atoms.

NPC structures are non-equilibrium and therefore, are dependent on the initial structure and processing conditions. This is observed in experimental NPCs where the temperature of pyrolysis is the primary governing factor for determining the degree of order and other material properties. Since a mimetic algorithm is being used in this work to generate model NPC structures, a trend similar to experiments is observed whereby the structure becomes kinetically trapped in a local free energy minimum after sufficient pyrolysis time. The results in the following paragraphs show that the final structure is nearly independent of the simulation parameters, such as simulation box size, starting configuration and random number sequence. However, the NPC structures do depend strongly on the thermodynamic variables like temperature and density.

Fig. 6(a) shows the change in the PDF as the structure evolves from an amorphous linear polymer to an amorphous carbon with interconnected graphene sheets. As the simulation progresses, the degree of correlation in the structure increases and the final structure obtained after 4000 MC cycles shows correlations out to 10 Å. A comparison of the PDF of this model carbon is made with the PDF of a real amorphous carbon (prepared at 800 °C) obtained by Petkov et al. [7] in Fig. 6(b). The two PDFs are in semi-quantitative agreement and their peak positions match closely. The bond anisotropy maps of the model carbon at different points in its evolution during the simulation, shown in Fig. 7, complement the information provided by the change in the PDFs with simulation progress. The starting polymer is amorphous and there is very little anisotropy with

respect to the bond directionality. As the simulation progresses, many bonds tend to preferentially orient along some specific directions leading to an increase in the anisotropy of the structure. This is characteristic of organization into graphene sheets.

The CSD of the final structure, shown in Fig. 8(a), indicates that there is a low but finite probability of inserting a nitrogen or an oxygen molecule into the structure. The EVM generated by using a hard sphere representation of oxygen molecule as probe (Fig. 8(c)) shows that there are regions within the structure where an oxygen molecule can be accommodated. The EVM generated by inserting a hard sphere representation for a nitrogen molecule (diameter = 3.70 Å) shows that nitrogen can be successfully inserted into the structure, but such regions are smaller than those observed for a hard sphere oxygen (diameter = 3.46 Å). A helium atom (diameter = 2.58 Å), which the cavity size distribution shows to have a much higher insertion probability than oxygen and nitrogen, does in fact see a larger free volume inside the carbon structure as shown in Fig. 8(b). Although an effective hard sphere representation of O₂ and N₂ has been used to calculate the EVMs, the molecules are anisometric and so, the actual insertion probabilities may be higher. The O₂ molecule whose effective hard sphere diameter is 3.46 Å has a dimension of 3.03 Å along the direction normal to the O–O bond.

Fig. 9 shows a comparison between the experimental TEM image [30] of an NPC prepared at 800 °C ($\rho = 1.72 \text{ g/cm}^3$) and the simulated TEM image of a model carbon (simulation 1 in Table 2). Similar level of organization of the carbon is observed in simulation and experiment.

Simulations were carried out at several other conditions of temperature, density, box size and starting

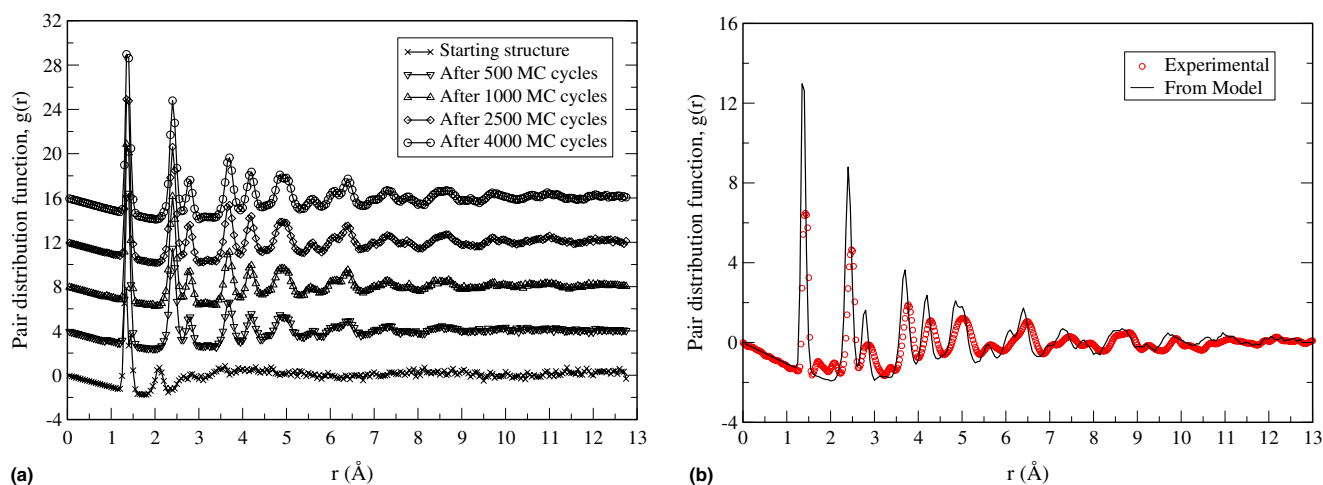


Fig. 6. PDF for structures generated by simulation at a temperature of 800 °C and a density of 1.72 g/cm^3 in a cubic simulation box of length 25.68 Å and having 1450 carbon atoms. (a) Change in the PDF as the structure evolves during the MC simulation (for comparison, the PDF of the final structure has also been shown). Some PDFs have been shifted vertically for clarity (b) a comparison of the PDF of the final structure with that of an experimental carbon ($\rho = 1.72 \text{ g/cm}^3$, prepared at 800 °C by Petkov et al. [7]).

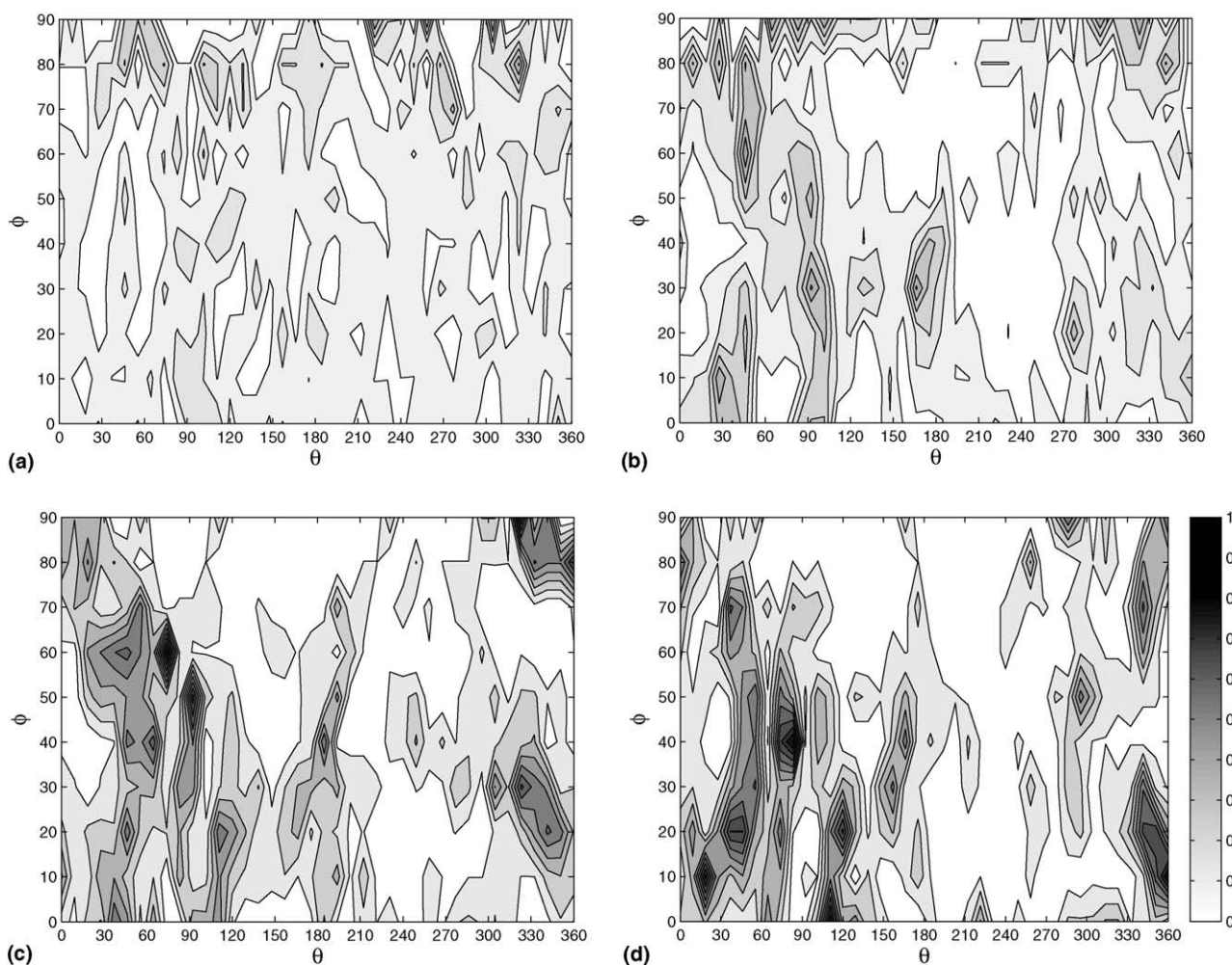


Fig. 7. Change in anisotropy of the carbon structure ($T = 800\text{ }^{\circ}\text{C}$ and $\rho = 1.72\text{ g/cm}^3$) as it evolves during the MC simulation: (a) Starting polymer, (b) after 100 MC cycles, (c) after 1000 MC cycles, (d) after 4000 MC cycles. The contour plots have been normalized by the maximum bond density in the structure obtained at the end of the simulation. The scale bar in (d) is common to all the contour plots.

structure to study the effects that these parameters have on the structure of the final carbon models obtained. To understand the effect the starting structure has on the carbons generated, two polymers (which will be referred to as polymer A and B) with different polymer lattice backbones (see Fig. 2(a)) were used as starting structures. These polymers were obtained by selecting two independent structures along the Monte Carlo trajectory of the algorithm used for polymer generation [31]. A third structure composed of a random arrangement of non-bonded carbon atoms was used as starting structure for a separate simulation. Finally, a fourth simulation was performed in which the random number generation sequence for the MC moves was altered with polymer A as the starting structure. All four of these simulations were carried out at a temperature of $800\text{ }^{\circ}\text{C}$, density of 1.72 g/cm^3 and a box size of 25.68 \AA . Fig. 5 shows the variation of fractions of carbon atoms having 1, 2 and 3 carbon atom neighbors with the number of MC cycles for three of the aforementioned simulations (simulations

1, 2 and 4 from Table 3; the results for simulation 3 are not shown here for clarity). The trend of the variation as well as the final values after 4000 MC cycles are very similar for all the three cases; the results for the fourth case (free carbon gas, simulation 3) were also found to be similar. The fractions of 5-, 6- and 7-membered rings in the final structure are comparable for the four cases as can be seen from Table 3. These results indicate that the starting structure as well as the random number generation sequence do not have an effect on the final structure.

On the other hand, the CSDs for these four cases, shown in Fig. 10(d), suggest that all these carbon structures have comparable insertion probabilities for helium. However, the structure generated using polymer B as the starting structure exhibits larger cavities than observed in the other three. Consequently, the probability for successfully inserting nitrogen and oxygen molecules is highest for the carbon generated from polymer B. The EVMs shown in Fig. 11 were generated using

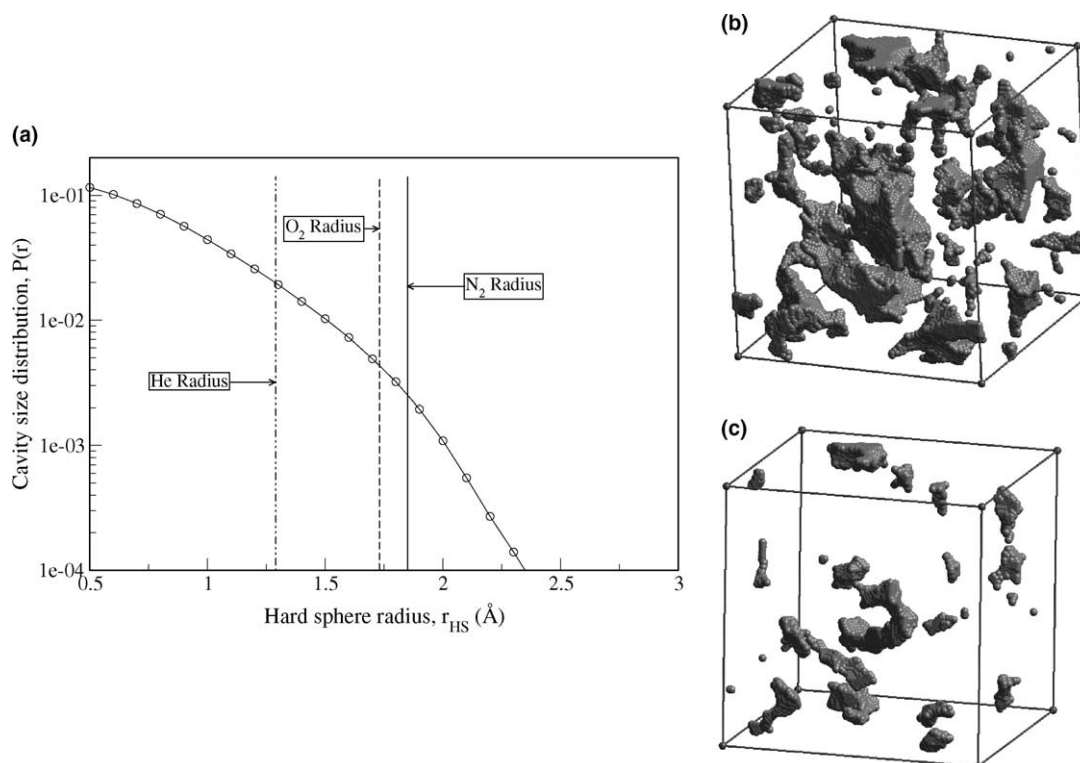


Fig. 8. CSD and EVMs for model structures generated by simulation at a temperature of 800 °C and a density of 1.72 g/cm³ in a cubic simulation box of length 25.68 Å and having 1450 carbon atoms. (a) CSD of the final structure. The vertical lines show the effective hard sphere radius of a helium atom ($r_{He} = 1.29$ Å), a nitrogen molecule ($r_{N_2} = 1.85$ Å) and an oxygen molecule ($r_{O_2} = 1.73$ Å). (b) EVM for the final structure obtained by inserting a hard sphere helium atom ($r_{He} = 1.29$ Å) and (c) EVM by inserting a hard sphere oxygen molecule ($r_{O_2} = 1.73$ Å).

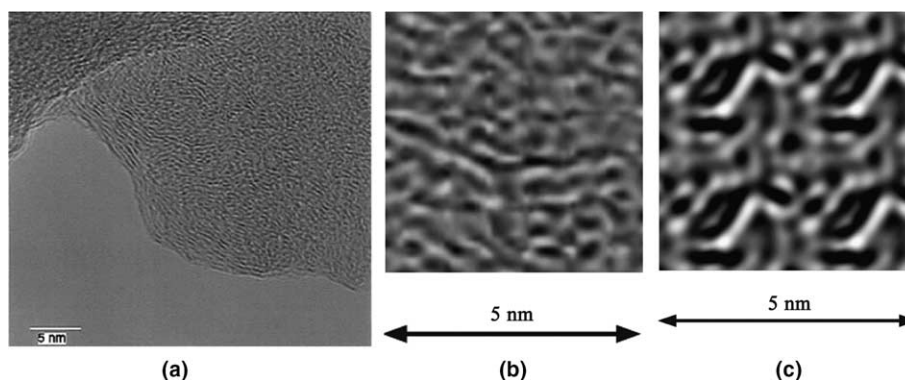


Fig. 9. Comparison of the experimental TEM image of an NPC prepared at 800 °C ($\rho = 1.72$ g/cm³) with the simulated TEM image of a model carbon (simulation 1 in Table 2). (a) Experimental TEM image [30], (b) magnified view of a portion of the experimental TEM image and (c) simulated TEM image.

helium insertion into the final amorphous carbons obtained for the four cases mentioned above. A helium atom “sees” large void spaces in all the structures and the amount of free volume experienced by a helium atom is quite similar for all four cases. Finally, the bond anisotropy maps in Fig. 12 for the final structures obtained in the above four cases show the presence of anisotropy in all four structures. Although the phenomenon of preferential orientation of bonds in some specific directions is observed in all four cases, the

direction in which this bond alignment takes place is very different. From the results presented above, it becomes evident that the starting structure does not have a big effect on the model amorphous carbons obtained in terms of the average structure and chemical composition, but the local orientation of bonds and structure of the “pore” space available for oxygen/nitrogen adsorption and diffusion depend on the initial structure. Consequently, we can conclude that the simulations are generating robust, representative NPC structures, but

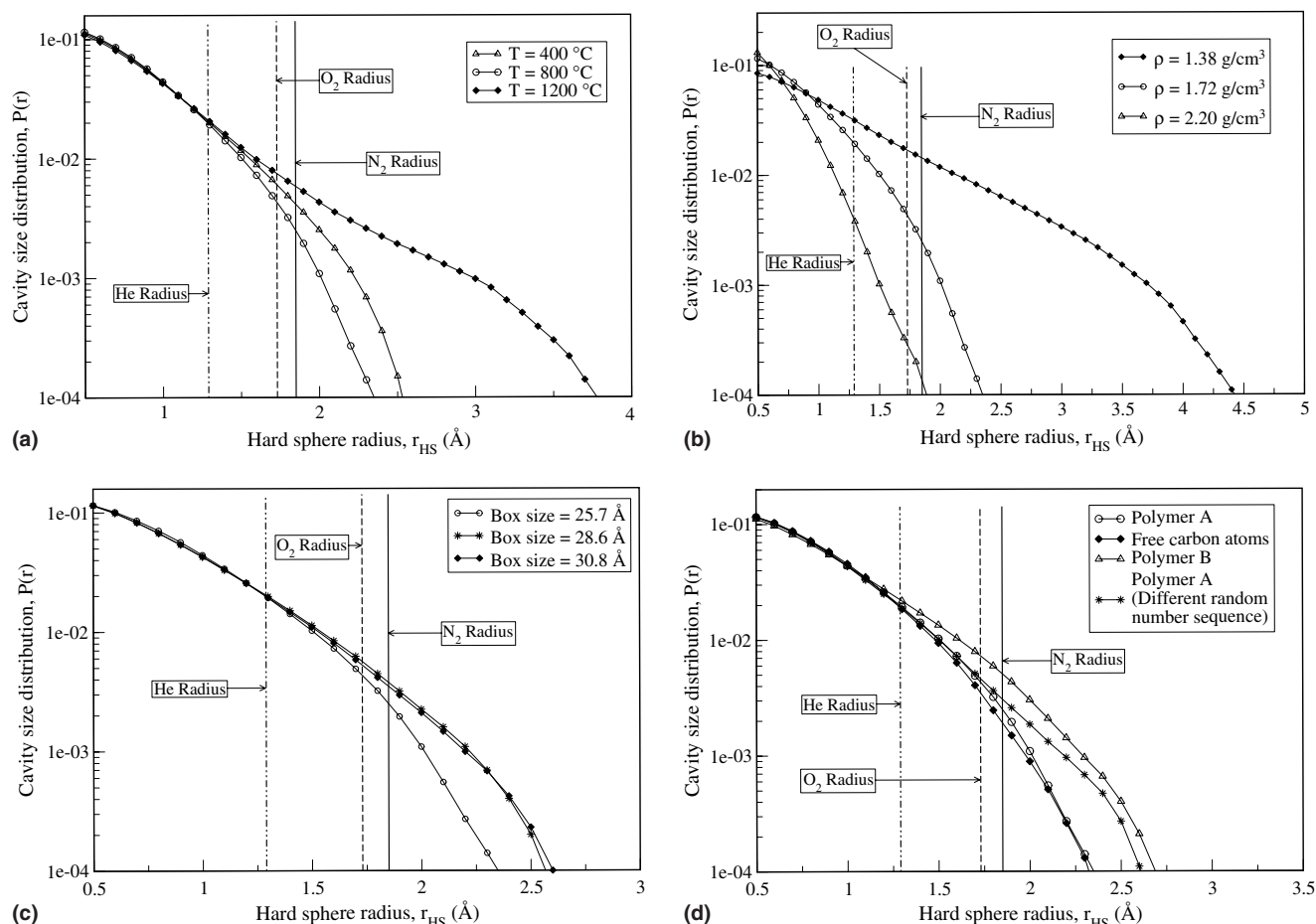


Fig. 10. Effect of change in (a) temperature, (b) density, (c) box size, and (d) starting structure on the CSD of the final structure obtained.

that the simulation size is too small such that fluctuations between systems are not negligible, as is often the case with molecular simulations.

Simulations were performed at three different temperatures (400°C , 800°C and 1200°C) keeping the other adjustable parameters constant ($\rho = 1.72\text{ g/cm}^3$, box size = 25.68 \AA , starting structure: Polymer A). The fractions of 5-, 6- and 7-membered rings are similar as can be seen from Table 3 (simulations 1, 5 and 6). The percentage of carbons bonded to three carbons increases with simulation temperature from 67% at 400°C to 74% at 1200°C (and consequently the percentage of hydrogen atoms goes down from 25% at 400°C to 21% at 1200°C). The CSD does not show any trend with simulation temperature as can be seen from Fig. 10(a). The structure obtained at 800°C has the smallest cavities and the lowest insertion probabilities for nitrogen and oxygen molecules and that obtained at 1200°C shows the presence of some very large cavities (larger than 3.5 \AA in radius). From the results, it can be concluded that the average structure is not affected by changes in simulation temperature at constant density, but rather the chemical composition

tends toward pure carbon with increasing pyrolysis temperature.

Simulations were also performed at three different densities (1.38 g/cm^3 , 1.72 g/cm^3 and 2.20 g/cm^3) keeping the other parameters constant ($T = 800^\circ\text{C}$, box size = 25.68 \AA , starting structure: Polymer A) to assess the effect of system density on the NPC structure. The fractions of 5-, 6- and 7-membered rings are similar for $\rho = 1.38\text{ g/cm}^3$ and $\rho = 1.72\text{ g/cm}^3$, however the simulation at $\rho = 2.20\text{ g/cm}^3$ has a significantly higher fraction of hexagonal rings as can be seen from Table 3 (simulations 1, 7 and 8). The percentage of carbon atoms bonded to three carbon atoms goes down with the density of the system from 73.48% at 1.38 g/cm^3 to 70.67% at 2.20 g/cm^3 (and consequently the percentage of hydrogen atoms goes up from 21.18% at 1.38 g/cm^3 to 22.96% at 2.20 g/cm^3). A wide difference is seen in the cavity size distribution of the final structures obtained for these three cases (Fig. 10(b)). Not unexpectedly, the probability of hard sphere insertion as well as the size of the cavities go up significantly as the density goes down. The system with the lowest density has cavities larger than 4 \AA in radius while the system with the

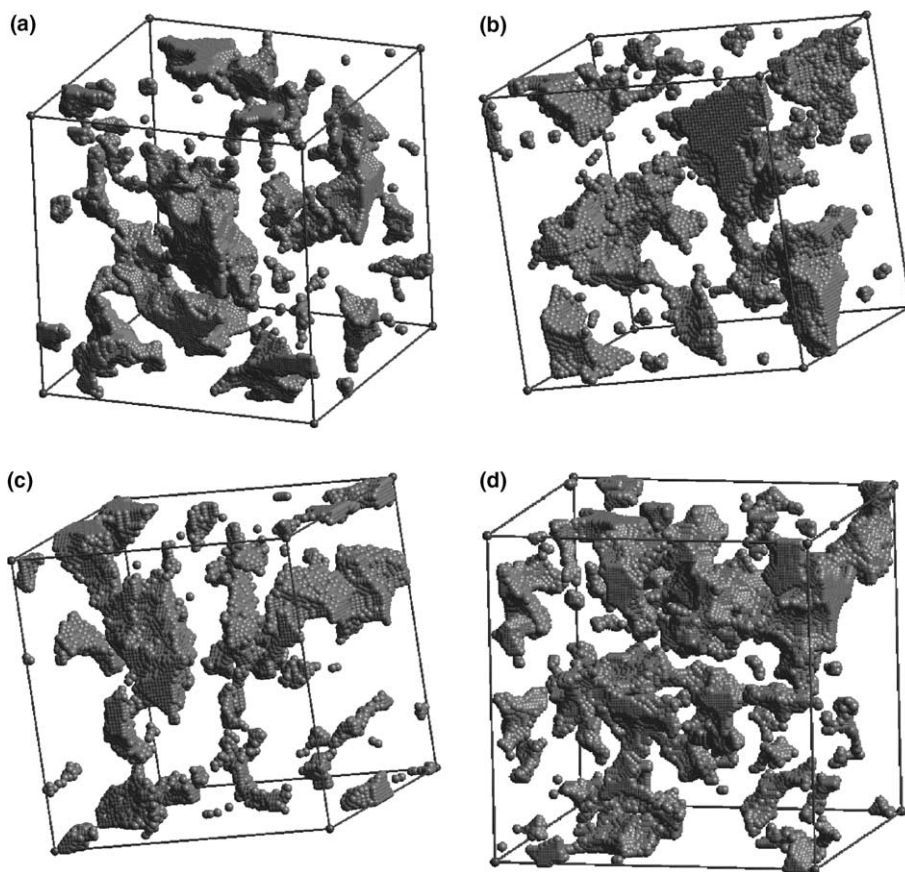


Fig. 11. Effect of change in starting structure on the EVMs obtained by helium insertion: (a) Polymer A, (b) polymer B, (c) polymer A (different sequence of random numbers) and (d) a (hypothetical) gas of free carbon atoms. Polymers A and B have the same number of carbon atoms but differ in conformation. The simulations were carried out at a temperature of 800 °C and a density of 1.72 g/cm³ in a cubic simulation box of length 25.68 Å and having 1450 carbon atoms.

largest density hardly has any cavities that can accommodate nitrogen.

Finally, the effect of simulation box size on the carbon structures was studied by using simulations with sizes 25.68 Å, 28.60 Å and 30.80 Å keeping the other parameters constant ($T = 800$ °C, $\rho = 1.72$ g/cm³, starting structure: Polymer A). The fractions of 5-, 6- and 7-membered rings are quite similar for all the three cases as can be seen in Table 3 (simulations 1, 9 and 10). The fraction of carbon atoms bonded to three carbon atoms in the final structure was also found to be similar for all three box sizes. The CSD shown in Fig. 10(c) indicates that the size of the cavities increases as the size of the simulation box is changed from 25.68 Å to 28.60 Å but does not change with further increase in the box size.

The results outlined in this section indicate that although the methodology to generate amorphous carbon models creates structures that are chemically sound and in good agreement with some experimental results, there are some inherent limitations. An important result is the presence of anisotropy in the model carbons. Experimental evidence [11] suggests that non-graphitizing carbons are generally isotropic. The net bond orien-

tation observed in our models is a consequence of the limited simulation size. No preference for this orientation is observed in independent simulations, suggesting it is not an artifact of the algorithm. HRTEM images [9,10] of amorphous carbons also show the presence of onion-like regions having predominantly positive curvature. The models presented in this work have similar amounts of pentagonal and heptagonal rings (which are responsible for the positive and negative curvatures respectively) implying that the overall average curvature is small. This is not surprising since the methodology used involves single-atom bond rearrangements while the mechanism of pyrolysis of polycyclic aromatic hydrocarbons, for example, involves steps like ring contraction and hydrogen shift [37]. The complex and poorly understood mechanism of PFA pyrolysis can also be expected to involve some similar multiple bond-breaking, bond-making steps.

These observations indicate several directions that can be followed to improve the agreement between models and real carbons. Multiple atom moves can be included in the algorithm to create more pentagonal rings at the expense of hydrogen atoms. Incorporating

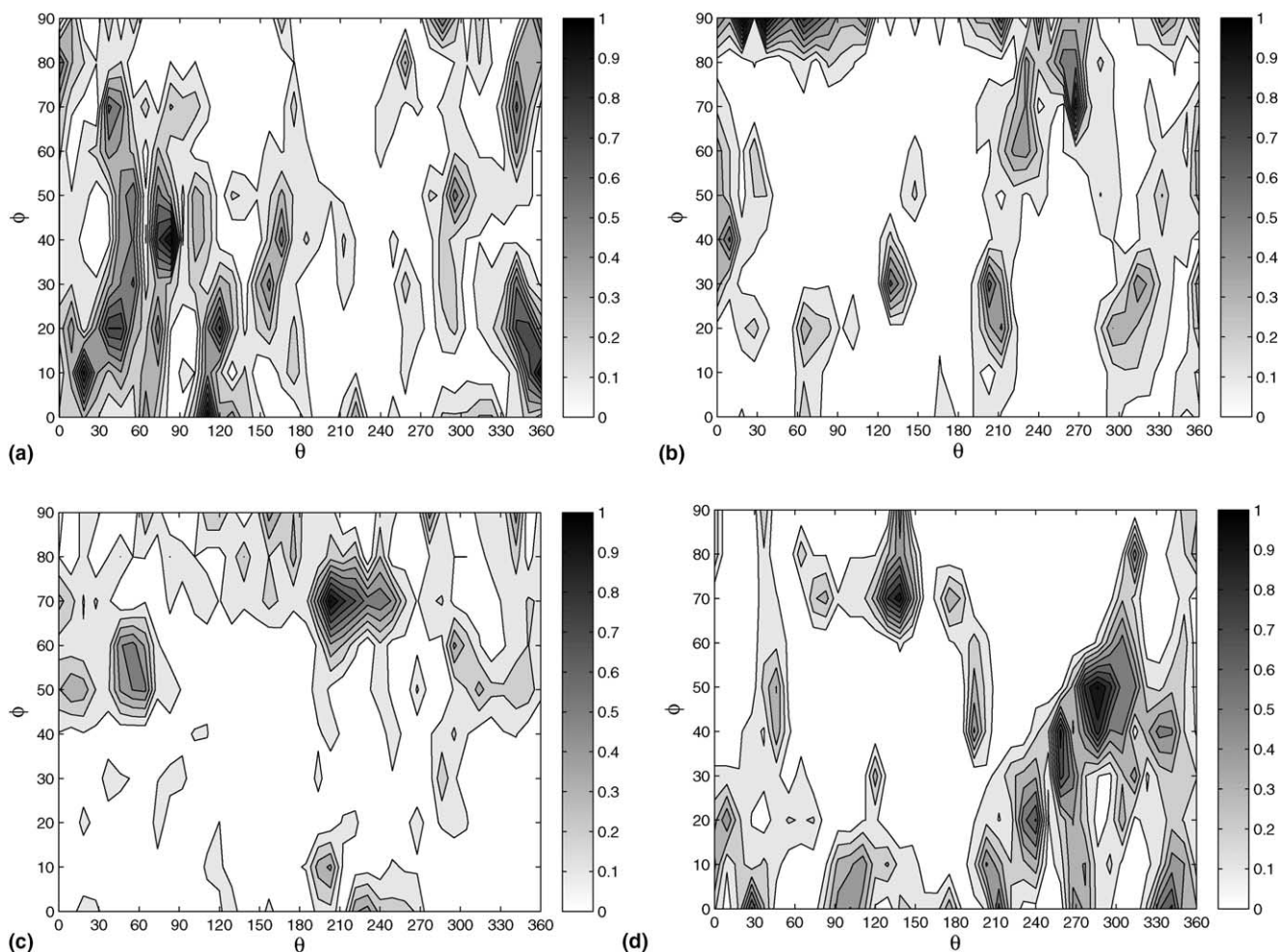


Fig. 12. Anisotropy maps for model carbons generated from different starting structures (a) Polymer A, (b) polymer B, (c) polymer A (different sequence of random numbers) and (d) free carbon atoms. Polymers A and B have the same number of carbon atoms but differ in conformation. The simulations were carried out at a temperature of 800 °C and a density of 1.72 g/cm³ in a cubic simulation box of length 25.68 Å and having 1450 carbon atoms.

such moves will serve to increase the fraction of 5-membered rings relative to the 7-membered rings resulting in more positive curvature in the structure. Removal of hydrogen atoms will also serve to bring the fraction of hydrogen atoms close to the experimentally observed value of 6–12%. Moreover, the creation of net positive curvature in the structure might reduce the observed anisotropy in the carbon models.

5. Conclusions

The new algorithm presented here is able to generate carbon structures that are amorphous, periodic and have the correct chemistry and density of real amorphous carbons. Our results indicate that the size of cavities in the final structure are most sensitive to the system density while the fraction of hydrogen atoms in the system is most sensitive to the simulation temperature. As the carbon structures evolve during the simu-

lation, they become more ordered and develop anisotropy. The starting structure used in the simulations does not have a significant effect on any of the important properties of the final carbons obtained. The CSD of the carbons indicated that the most relevant structures contain sites for molecular nitrogen and oxygen adsorption. These model NPC structures are currently being used to study sorption and molecular transport for understanding the remarkable gas separation selectivities of NPCs.

Acknowledgements

This work was supported by NSF Grant No. EEC-0085461. Useful discussions with Dr. Jan H. D. Boshoff about the MC simulations and with Dr. Michael A. Smith are gratefully acknowledged. We would also like to thank Dr. Henry C. Foley for providing the TEM image.

References

- [1] Franklin RE. Crystallite growth in graphitizing and non-graphitizing carbons. *Proc Roy Soc London Series A—Math Phys Sci* 1951;209:196–218.
- [2] Rao MB, Sircar S. Performance and pore characterization of nanoporous carbon membranes for gas separation. *J Membr Sci* 1996;110:109–18.
- [3] Lee JJ, Han S, Kim H, Koh JH, Hyeon T, Moon SH. Performance of CoMoS catalysts supported on nanoporous carbon in the hydrodesulfurization of dibenzothiophene and 4,6-dimethyldibenzothiophene. *Catal Today* 2003;86:141–9.
- [4] Strano MS, Foley HC. Synthesis and characterization of heteropolyacid nanoporous carbon membranes. *Catal Lett* 2001;74:177–84.
- [5] Ruthven DM, Farooq S, Knaebel KS. *Pressure swing adsorption*. New York: VCH publishers inc.; 1993.
- [6] Shiflett MB, Foley HC. Ultrasonic deposition of high-selectivity nanoporous carbon membranes. *Science* 1999;285:1902–5.
- [7] Petkov V, DiFrancesco RG, Billinge SJL, Acharya M, Foley HC. Local structure of nanoporous carbons. *Philos Mag B* 1999;79:1519–30.
- [8] Mariwala RK, Foley HC. Calculation of micropore sizes in carbogenic materials from the methyl-chloride adsorption-isotherm. *Ind Eng Chem Res* 1994;33:2314–21.
- [9] Kane MS, Foley HC. Local microstructural organization in carbogenic molecular sieves. In: *Materials Research Society Symposium*. vol. 431. Materials Research Society; 1996. p. 9–14.
- [10] Harris PJF, Tsang SC. High-resolution electron microscopy studies of non-graphitizing carbons. *Philos Mag A* 1997;76:667–77.
- [11] Harris PJF, Burian A, Duber S. High-resolution electron microscopy of a microporous carbon. *Philos Mag Lett* 2000;80:381–6.
- [12] Gelb LD, Gubbins KE. Characterization of porous glasses: simulation models, adsorption isotherms and the Brunauer–Emmett–Teller analysis method. *Langmuir* 1998;14:2097–111.
- [13] Feuston BP, Higgins JB. Model structures for MCM-41 materials: a molecular dynamics simulation. *J Phys Chem* 1994;98:4459–62.
- [14] Benoit M, Ispas S, Jund P, Jullien R. Model of silica glass from combined classical and ab initio molecular-dynamics simulations. *Eur Phys J B* 2000;13:631–6.
- [15] McGreevy RL, Pusztai L. Reverse Monte Carlo simulation: A new technique for the determination of disordered structures. *Mol Sim* 1988;1:359–67.
- [16] Thomson KT, Gubbins KE. Modeling structural morphology of microporous carbons by reverse Monte Carlo. *Langmuir* 2000;16:5761–73.
- [17] Pikunic J, Clinard C, Cohaut N, Gubbins KE, Guet JM, Pellenq RJM, et al. Structural modeling of porous carbons: constrained reverse Monte Carlo method. *Langmuir* 2003;19:8565–82.
- [18] Keen DA, McGreevy RL. Structural modeling of glasses using reverse Monte-Carlo simulation. *Nature* 1990;344:423–5.
- [19] Wicks JD, Börjesson L, Bushnell-Wye G, Howells WS, McGreevy RL. Structure and ionic conduction in $(AgI)_x(AgPO_3)_{1-x}$ glasses. *Phys Rev Lett* 1995;74:726–9.
- [20] Cormier L, Gaskell PH, Calas G, Zhao J, Soper AK. Environment around Li in the $LiAlSiO_4$ ionic conductor glass: a neutron-scattering and reverse Monte Carlo study. *Phys Rev B* 1998;57:R8067–70.
- [21] Hoppe U, Kranold R, Stachel D, Barz A, Hannon AC. A neutron and X-ray diffraction study of the structure of the LaP_3O_9 glass. *J Non-Cryst Solids* 1998;232–234:44–50.
- [22] Warren BE. X-ray diffraction study of carbon black. *J Chem Phys* 1934;2:551–5.
- [23] Warren BE. X-ray diffraction in random layer lattices. *Phys Rev* 1941;59:693–8.
- [24] Acharya M, Strano MS, Mathews JP, Billinge SJL, Petkov V, Subramoney S, et al. Simulation of nanoporous carbons: a chemically constrained structure. *Philos Mag B* 1999;79:1499–518.
- [25] Smith MA, Foley HC, Lobo RF. A simple model describes the PDF of a non-graphitizing carbon. *Carbon* 2004;42:2041–8.
- [26] Rosato V, Lascovich JC, Santoni A, Colombo L. On the use of reverse Monte Carlo technique to generate amorphous carbon structures. *Int J Mod Phys C* 1998;9:917–26.
- [27] Harris PJF. Structure of non-graphitizing carbons. *Int Mater Rev* 1997;42:206–18.
- [28] Bandosz TJ, Biggs MJ, Gubbins KE, Hattori Y, Iiyama T, Kaneko K, et al. Molecular models of porous carbons. In: Radovic LR, editor. *Chemistry and physics of carbon*, vol. 28. Marcel Dekker; 2003. p. 41–228.
- [29] Shiflett MB, Foley HC. Reproducible production of nanoporous carbon membranes. *Carbon* 2001;39:1421–5.
- [30] Kane MS, Goellner JF, Foley HC, DiFrancesco R, Billinge SJL, Allard LF. Symmetry breaking in nanostructure development of carbogenic molecular sieves: Effects of morphological pattern formation on oxygen and nitrogen transport. *Chem Mater* 1996;8:2159–71.
- [31] Kotelyanskii M, Wagner NJ, Paulaitis ME. Building large amorphous polymer structures: atomistic simulation of glassy polystyrene. *Macromolecules* 1996;29:8497–506.
- [32] Mayo SL, Olafson BD, Goddard WA. DREIDING: a generic force-field for molecular simulations. *J Phys Chem* 1990;94:8897–909.
- [33] Allen MP, Tildesley DJ. *Computer simulation of liquids*. Oxford: Oxford University Press; 1987.
- [34] *Molecular simulations*. San Diego. Cerius² modeling environment; 1997.
- [35] Keen DA. A comparison of various commonly used correlation functions for describing total scattering. *J Appl Crystallogr* 2001;34:172–7.
- [36] Cuthbert TR, Wagner NJ, Paulaitis ME, Murgia G, D’Aguanno B. Molecular dynamics simulation of penetrant diffusion in amorphous polypropylene: diffusion mechanisms and simulation size effects. *Macromolecules* 1999;32:5017–28.
- [37] Necula A, Scott LT. High temperature behavior of alternant and nonalternant polycyclic aromatic hydrocarbons. *J Anal Appl Pyrol* 2000;54:65–87.